

Electronic Raman scattering in superconductors on triangle lattices

Jian-Bo Wang, Xiang-Mei He, Fei Tan, and Qiang-Hua Wang

National Laboratory of Solid State Microstructures, Nanjing University, Nanjing 210093, China

In superconductors on triangle lattices, we show that the electronic Raman spectra in the non-resonant channel are independent of the light polarization configuration in the scattering. Therefore the light polarization configuration is no longer a judicious choice to probe the anisotropic nature of the pairing wave function (as in the case of square lattices). However, we show that the detailed energy-shift dependence of the spectrum and the effects of impurities provide useful information that can help identify the possible pairing symmetry experimentally. These results are relevant to the newly discovered $\text{Na}_x\text{CoO}_2 \cdot y\text{H}_2\text{O}$ superconductors.

The electronic Raman scattering in the so-called non-resonant channel (without invoking inter-band scattering) measures the fluctuations of the effective density operator $\rho_{\mathbf{q}} = \sum_{\mathbf{k}\sigma} \gamma_{\mathbf{k}} C_{\mathbf{k}+\mathbf{q}\sigma}^\dagger C_{\mathbf{k}\sigma}$ in the limit of $\mathbf{q} \rightarrow 0$ (In the scattering event, \mathbf{q} is the momentum transfer from the lights, which is vanishingly small compared to the Fermi momentum.) Here $\gamma_{\mathbf{k}}$ is the Raman vertex that describes the diamagnetic second-order coupling between electrons and lights, $\gamma_{\mathbf{k}} = (\mathbf{e}_i \cdot \nabla_{\mathbf{k}})(\mathbf{e}_s \cdot \nabla_{\mathbf{k}})\epsilon_{\mathbf{k}}$, where \mathbf{e}_i and \mathbf{e}_s are the polarization directions of the incident and scattered lights, and $\epsilon_{\mathbf{k}}$ is the normal state dispersion. The Raman response function $\chi(\mathbf{q}, \omega)$, with $\omega = \omega_i - \omega_s$ being the energy transfer in the scattering, is the Fourier transform of the retarded Green's function $\chi(\mathbf{q}, t) = -i\langle[\rho_{\mathbf{q}}(t), \rho_{-\mathbf{q}}(0)]\rangle\theta(t)$. The Raman intensity (*RI*) is eventually given by $-\text{Im}[\chi(\mathbf{q} \rightarrow 0, \omega)]$. Theoretically, $\chi(\mathbf{q}, \omega)$ can be conveniently obtained from the analytical continuation of the Matsubara propagator $\chi(\mathbf{q}, i\omega_n \rightarrow \omega + i0^+)$.

The electronic Raman response vanishes in ideal metals because of lack of phase space for finite-energy and zero-momentum particle-hole excitations, but is finite in a superconductor because a Cooper pair can be broken with no change in the center-of-mass momentum. By adjusting the incident and scattered photon polarizations, through the Raman vertex function Raman scattering may projects out various parts of the quasi-particle excitations in the momentum space, and is therefore highly useful to probe the angular dependence of the possible anisotropic pairing wave function on the Fermi surface. This has been applied very successfully in cuprate superconductors.[1] Because of the square lattice of the copper oxide plane, there are two Raman-active anisotropic channels, *i.e.*, the B_{1g} and B_{2g} channels. These channels can be conveniently picked up by adjusting the polarizations of the incident and scattered lights. The fact that the Raman responses are different in these channels is a proof that the pairing wave function is anisotropic, and is consistent with the *d*-wave symmetry. Furthermore, the detailed energy-dependence of the response yield useful information on the dynamics of the quasi-particles. It is therefore natural to explore how electronic Raman scattering can be used in super-

conductors on other lattices.

In this paper, we shall concentrate on triangle lattices, motivated by the discovery of the $\text{Na}_x\text{CoO}_2 \cdot y\text{H}_2\text{O}$ superconductor,[2] which does have triangular CoO_2 layers, separated by thick insulating layers of Na^+ ions and H_2O molecules. The two-dimensional layered structure is similar to the copper oxide and it is conjectured that a similar superconductivity mechanism may be at work. In particular, it is argued that this is a doped Mott insulator that would be described by the resonant-valence-bond (RVB) theory.[3] In such a scenario, the pairing symmetry would be $d_{x^2-y^2} + id_{xy}$ with a full energy gap for quasi-particle excitations. On the other hand, given the experimental fact that the parent compounds exhibit intra-plane ferromagnetic correlations, $p_x + ip_y$ - [4] or *f*-wave [5] pairing symmetries are also proposed as possible candidates. For these triplet channels, the *p*-wave pairing has a full gap, while the *f*-wave pairing have nodal lines in the gap function. Finally, if the pairing is due to lattice vibrations, an *s*-wave gap function is to be expected. As an important step toward understanding the pairing mechanism, one is therefore asked to discriminate experimentally one from the others in this list of possible pairing symmetries.

Existing experimental data are still controversial. From nuclear-magnetic-resonance (NMR) measurements, Kato *et al* proposed *p*-wave triplet pairing,[6] while Kobayashi *et al* conjectured *s*-wave singlet pairing.[7] Nonetheless, from the coherence peak in the temperature dependence of the spin-lattice relaxation rate $1/T_1$ both groups agreed that the gap has no nodal lines. This is to be contrasted to the evidence of nodal lines in nuclear-quadruple-resonance (NQR) data [8] and in the specific heat measurement.[9] The main difficulty for all measurements is the control of the sample quality, and it is quite likely the reason behind the inconsistency of the experimental results. While this asks for better sample quality to resolve the inconsistency, in this paper we propose electronic Raman scattering as additional but important probe to the pairing symmetry. We note, however, that the low transition temperature (about 4.5K) may impose a difficulty for the measurement of the pairing gap due to the laser heating effect. Our hope is that the technical

difficulty could be removed and that samples with higher transition temperatures could be achieved.

The structure of the rest of the paper is as follows. We first analyze the Raman response in the clean system, reaching the result that the response is independent of the polarization configuration of the scattering. We show the result by explicit calculation of a lattice model, and substantiate by a proof in the continuum limit. The Raman response in the clean system can only tell whether there is a full gap on the Fermi surface. Second, the effect of impurity is taken into account. We find that the impurity effects do not induce Raman absorption below the pair breaking peak (PBP) for s -wave pairing, while they do so for $p_x + ip_{y-}$ and $d_x^2 - y^2 + id_{xy}$ -wave pairing. We also find a universal Raman response in the case of nodal f -wave pairing in the limit of small Raman energy shift for small scattering rates. Combined with a probe to the singlet versus triplet pairing, these features enables one to identify the pairing symmetry unambiguously.

We start from the effective mean field Hamiltonian,

$$H = \sum_{\mathbf{k}\sigma} \epsilon_{\mathbf{k}} C_{\mathbf{k}\sigma}^\dagger C_{\mathbf{k}\sigma} + \sum_{\mathbf{k}} (\Delta_{\mathbf{k}} C_{\mathbf{k}\uparrow}^\dagger C_{-\mathbf{k}\downarrow}^\dagger + \text{h.c.}), \quad (1)$$

where $\epsilon_{\mathbf{k}} = -2t \sum_{i=1}^3 \cos \mathbf{k} \cdot \delta_i - \mu$. Here $\delta_{1,2,3} = (1, 0)$, $(1/2, \sqrt{3}/2)$ and $(-1/2, \sqrt{3}/2)$ are three unit vectors on the triangle lattice, μ is the chemical potential. For the $\text{Na}_x\text{CoO}_2 \cdot y\text{H}_2\text{O}$ superconductor, band structure calculation reveals a large hole pocket around the Γ point in the momentum space,[10] it is therefore consistent to take $t < 0$ in the dispersion. We also tune the chemical potential so that there are 1.35 electrons per site. $\Delta_{\mathbf{k}}$ is the pairing gap function. For the s -, $p_x + ip_{y-}$, $d_{x^2-y^2} + id_{xy}$ - and f -wave pairing symmetries, the gap functions we will consider are, respectively,

$$\Delta_{\mathbf{k}}^s = \Delta \sum_{i=1}^3 \cos \mathbf{k} \cdot \delta_i; \quad (2)$$

$$\Delta_{\mathbf{k}}^p = \Delta \sum_{i=1}^3 \sin(\mathbf{k} \cdot \delta_i) \exp(i\theta_i); \quad (3)$$

$$\Delta_{\mathbf{k}}^d = \Delta \sum_{i=1}^3 \cos(\mathbf{k} \cdot \delta_i) \exp(2i\theta_i); \quad (4)$$

$$\Delta_{\mathbf{k}}^f = \Delta \sum_{i=1}^3 \sin(\mathbf{k} \cdot \delta_i) \exp(3i\theta_i), \quad (5)$$

where $\theta_{1,2,3} = 0, \pi/3$ and $2\pi/3$ are the azimuthal angles of $\delta_{1,2,3}$, respectively. In the following calculation we take the gap amplitude as $\Delta = 0.1|t|$ for illustration purpose. The conclusion does not depend on this parameterization. We note that the gap on the Fermi surface is finite for the cases of s -, $p_x + ip_{y-}$, and $d_{x^2-y^2} + id_{xy}$ -wave cases, and it has nodal points for the f -wave pairing. The bare Matsubara propagator for the effective density $\rho_{\mathbf{q}}$ in the

limit of $\mathbf{q} = 0$ can be written as,

$$\chi_{\gamma\gamma}^0(i\nu_n) = -\frac{T}{N} \sum_{\mathbf{k}, i\omega_n} \text{Tr}[\gamma_{\mathbf{k}} \sigma_3 G(\mathbf{k}, i\omega_n) \gamma_{\mathbf{k}} \sigma_3 G(\mathbf{k}, i\omega_n + i\nu_n)], \quad (6)$$

where N is the number of lattice sites, and G is the mean field Green's function given by

$$G^{-1}(\mathbf{k}, i\omega_n) = i\omega_n \sigma_0 - \epsilon_{\mathbf{k}} \sigma_3 - (\Delta_{\mathbf{k}} \sigma^+ + \text{h.c.}). \quad (7)$$

Here ω_n and ν_n are Fermionic and Bosonic Matsubara frequencies, respectively, σ_0 is the 2×2 unitary matrix, $\sigma_{1,2,3}$ are the Pauli matrices, and $\sigma^+ = (\sigma_1 + i\sigma_2)/2$. The summation over Matsubara frequencies can be completed exactly. After the analytical continuation, we get the bare retarded Raman response function,

$$\chi_{\gamma\gamma}^0(\omega) = \frac{1}{N} \sum_{\mathbf{k}} \frac{\gamma_{\mathbf{k}}^2 |\Delta_{\mathbf{k}}|^2}{E_{\mathbf{k}}^2} \tanh \frac{\beta E_{\mathbf{k}}}{2} \times \left[\frac{1}{\omega - 2E_{\mathbf{k}} + i0^+} - \frac{1}{\omega + 2E_{\mathbf{k}} + i0^+} \right], \quad (8)$$

where $E_{\mathbf{k}} = \sqrt{\epsilon_{\mathbf{k}}^2 + |\Delta_{\mathbf{k}}|^2}$. In the limit where $\gamma_{\mathbf{k}} \sim 1$ the response function is equivalently a bare charge density susceptibility in the long wave length limit. However, in a charged system, the spectral weight of this susceptibility is pushed up to the plasma frequency. While this fact can be taken into account by a random-phase-approximation-like approach, the effect of Coulomb screening on the Raman response can be taken into account by simply projecting away the symmetrical part as follows[11]

$$\chi_{\gamma\gamma} = \chi_{\gamma\gamma}^0 - \frac{\chi_{\gamma_1}^0 \chi_{1\gamma}^0}{\chi_{11}^0}, \quad (9)$$

which is applicable below the plasma frequency. Here we suppressed the frequency arguments for brevity, and $\chi_{\gamma_1}^0$ and χ_{11}^0 are obtained by replacing $\gamma_{\mathbf{k}}$ by 1 for one or two of the Raman vertices in $\chi_{\gamma\gamma}^0$.

To proceed, we write according to the given definition the three typical Raman vertex functions in the xx , yy and xy polarization configurations as follows,

$$\gamma_{\mathbf{k}}^{xx} = 2t \left(\cos k_x + \frac{1}{2} \cos \frac{k_x}{2} \cos \frac{\sqrt{3}k_y}{2} \right); \quad (10)$$

$$\gamma_{\mathbf{k}}^{yy} = 3t \cos \frac{k_x}{2} \cos \frac{\sqrt{3}k_y}{2}; \quad (11)$$

$$\gamma_{\mathbf{k}}^{xy} = -\sqrt{3}t \sin \frac{k_x}{2} \sin \frac{\sqrt{3}k_y}{2}. \quad (12)$$

The vertex function for an arbitrary polarization configuration can be expressed in terms of the above as,

$$\gamma_{\mathbf{k}} = \cos \phi_i \cos \phi_s \gamma_{\mathbf{k}}^{xx} + \sin \phi_i \sin \phi_s \gamma_{\mathbf{k}}^{yy} + \sin(\phi_i + \phi_s) \gamma_{\mathbf{k}}^{xy}, \quad (13)$$

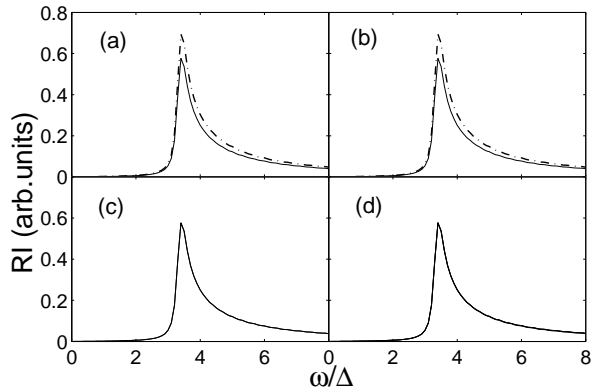


FIG. 1: The electronic Raman spectra for $p_x + ip_y$ -wave pairing in the (a) xx , (b) yy and (c) xy polarization configurations. The dashed (solid) lines denote the bare (screened) spectra. (d) is the screened spectra in the three configurations plot together. Note that in (c) the dashed line falls on top of the solid line and is therefore invisible.

where $\phi_{i,s}$ are the azimuthal angles of the polarizations of the incident and scattered lights, respectively.

With the above ingredients, we are now able to calculate the Raman spectra (the imaginary parts of $\chi_{\gamma\gamma}^0$ and $\chi_{\gamma\gamma}$) explicitly. We take the zero temperature limit in what follows. Fig.1 is the spectra for the $p_x + ip_y$ -wave pairing in the xx (a), yy (b) and xy (c) polarization configurations. The dashed (solid) lines denote the bare (screened) spectra. The PBP occurs near $\omega = 4\Delta$. This is because the effective gap on the Fermi surface is near 2Δ , and the major contribution to the summation over \mathbf{k} in χ^0 is from the region near the Fermi surface. It is clear that while the bare spectra depends on the polarization configurations, the screened ones do not, which is made clearer by plotting them together in Fig.1(d). This is true for any other arbitrary configurations (not shown here). Experimentally it is the screened spectra that are measured. We therefore conclude that the Raman spectra on triangle lattices are independent of the polarization configuration.

In order to understand the above result, it is useful to resort to symmetry analysis. In general, the Raman vertex function can be decomposed in terms of the basis function of the irreducible representations of the point group. For the system under concern, there are only two Raman-active irreducible representations, *i.e.*, the one-dimensional A_{1g} and two-dimensional E_g representations. The corresponding basis function for A_{1g} is

$$\gamma_a = \cos k_x + 2 \cos \frac{k_x}{2} \cos \frac{\sqrt{3}k_y}{2}, \quad (14)$$

and that for the E_g representation is $\gamma_e = (\gamma_{e1}, \gamma_{e2})$ with

$$\gamma_{e1} = \sqrt{3} \sin \frac{k_x}{2} \sin \frac{\sqrt{3}k_y}{2}; \quad (15)$$

$$\gamma_{e2} = \cos k_x - \cos \frac{k_x}{2} \cos \frac{\sqrt{3}k_y}{2}. \quad (16)$$

Symmetry arguments guarantee that the Raman response is also decomposed into these two channels. Furthermore, since γ_a has the full symmetry of the system itself, the Raman response in this channel will be screened. Therefore, E_g is the only channel for electronic Raman response, and this implies that at least the line shape of the Raman response should be independent of the polarization configuration as illustrated in Fig.1. It remains to be shown that even the amplitude of the Raman spectra is independent of the polarization configuration. We first verify the claim by taking advantage of the typical result in Fig.1, and then present a more rigorous proof by going to the continuum limit.

In terms of the basis functions, the three typical Raman vertex functions can be rewritten as,

$$\gamma^{xx} = t(\gamma_a + \gamma_{e2}); \quad (17)$$

$$\gamma^{yy} = t(\gamma_a - \gamma_{e2}); \quad (18)$$

$$\gamma^{xy} = -t\gamma_{e1}. \quad (19)$$

Since the γ_a component does not contribute to $\chi_{\gamma\gamma}$ due to screening, Fig.1 proves that the $\gamma_{e1,e2}$ components contribute equally to the $\chi_{\gamma\gamma}$, or $\chi_{\gamma_{e1}\gamma_{e1}} = \chi_{\gamma_{e2}\gamma_{e2}}$. Now consider an arbitrary vertex which can be rewritten as

$$\gamma = t(\cos \phi_{\gamma_{e1}} - \sin \phi_{\gamma_{e2}}), \quad (20)$$

where $\phi = \phi_i + \phi_f$, and we dropped the γ_a component, anticipating the screening effect. Consequently,

$$\chi_{\gamma\gamma} = \cos^2 \phi \chi_{\gamma_{e1}\gamma_{e1}} + \sin^2 \phi \chi_{\gamma_{e2}\gamma_{e2}} \equiv \chi_{\gamma_{e1}\gamma_{e1}}, \quad (21)$$

where a contribution from the crossing term $\gamma_{e1}\gamma_{e2}$ vanishes by symmetry.

To close the argument, we now prove $\chi_{\gamma_{e1}\gamma_{e1}} = \chi_{\gamma_{e2}\gamma_{e2}}$ for all of the pairing symmetries listed previously in the continuum limit. Since the screening effect is absent in the anisotropic E_g channel, it suffices to prove $\chi_{\gamma_{e1}\gamma_{e1}}^0 = \chi_{\gamma_{e2}\gamma_{e2}}^0$. Near the Fermi surface, one can write approximately but without loss of symmetry (up to trivial common factors),

$$\gamma_{e1} \sim \sin 2\theta; \quad \gamma_{e2} \sim \cos 2\theta, \quad (22)$$

where θ is the azimuthal angle of the Fermi momentum \mathbf{k}_F approximately on a circle. On the other hand, the gap functions can be approximated as

$$\Delta_\theta^s \sim \Delta_F, \quad (23)$$

$$\Delta_\theta^p \sim \Delta_F \exp(i\theta), \quad (24)$$

$$\Delta_\theta^d \sim \Delta_F \exp(2i\theta), \quad (25)$$

$$\Delta_\theta^f \sim \Delta_F \sin(3\theta), \quad (26)$$

where Δ_F is the effective gap amplitude on the Fermi surface for the specific cases. It is seen that $|\Delta_\theta|^2$ is

either a constant (for s -, $p_x + ip_y$ - and $d_{x^2-y^2} + id_{xy}$ -symmetries) or six-fold symmetric (for f -wave symmetry) on the Fermi surface, whereas $\gamma_{e1,e2}^2 = (1 \pm \cos 4\theta)/2$ which is four-fold symmetric. Plugging these into the expression for χ^0 and going over to the continuum limit, one concludes that by symmetry only the constant part in $\gamma_{e1,e2}^2$ contributes to the response function. This complete the prove. It is interesting to point out that in the case of $d_{x^2-y^2}$ -wave pairing on a square lattice, $\gamma_{e1,e2}$ becomes the basis functions for the B_{2g} and B_{1g} representations. In this case, $|\Delta_\theta|^2$ is four-fold symmetric, which can resonate with the corresponding component in $\gamma_{e1,e2}^2$, and this is why in that case the Raman spectra is different in B_{1g} and B_{2g} channels.

Having convinced ourselves that the Raman spectra on a triangle lattice do not depend on polarization configuration for all the relevant pairing symmetries, we now look into the energy dependence of the spectra. Fig.2 shows the screened Raman spectra for the four pairing symmetries under concern. As anticipated, the spectra have a threshold for the fully-gapped (a) s -, (b) $p_x + ip_y$ -, and (c) $d_{x^2-y^2} + id_{xy}$ -wave pairing, whereas it is linear at low energy for the nodal (d) f -wave pairing. The PBP in Fig.2 occur at different energies in units of Δ . This is again due to the fact that the effective gap amplitude Δ_F on the Fermi surface differs in the cases considered, even though the same Δ is used in the gap function. We also note that the line shape for the d -wave case is slightly different from the s - and p -wave cases. This is because the d -wave gap value under concern is close to the van-Hove singularity of the normal state density of states (DOS), which contributes a secondary peak near the threshold. We do not expect it to be a generic feature. In summary, in the clean system considered so far, the Raman spectra can only tell whether the pairing gap is nodal or not. However, impurities are always present in real systems, and it is pending to see whether impurity effects can help differentiate the three fully-gapped pairing cases. This is to be anticipated as impurities may induce low energy (Andreev) states for nontrivial pairing, even if it is fully gapped in the clean system. This will be discussed in the following.

The effect of impurities can be conveniently accounted for by the coherent potential approximation (CPA). The modified Green's function is determined by

$$G^{-1}(\mathbf{k}, i\omega_n) = i\omega_n\sigma_0 - \epsilon_{\mathbf{k}}\sigma_3 - (\Delta_{\mathbf{k}}\sigma^+ + \text{h.c.}) - \Sigma(\omega_n) \quad (27)$$

where $\Sigma(\omega_n) = \Sigma_0(\omega_n)\sigma_0 + \Sigma_1(\omega_n)\sigma_1$. Henceforth we apply the continuum limit and assume particle-hole symmetry near the Fermi surface so that the σ_3 component of Σ vanishes. We take $\Delta_{\mathbf{k}}^s$ to be real for definiteness. On the other hand, we anticipate that the $\sigma_{1,2}$ (or σ^\pm) components of Σ vanishes for pairing symmetries other than the s -wave, as to be verified hereafter. The self-energy Σ

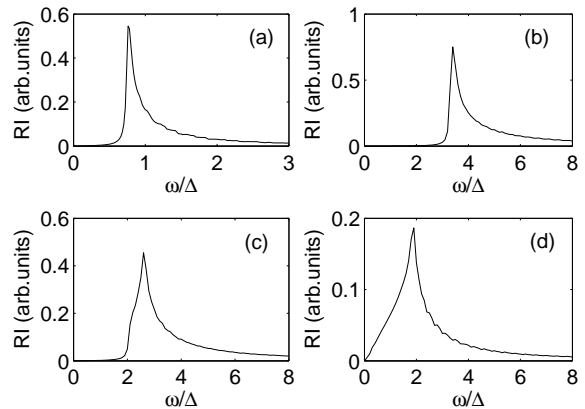


FIG. 2: The screened electronic Raman spectra for (a) s -, (b) $p_x + ip_y$ -, (c) $d_{x^2-y^2} + id_{xy}$ -, and (d) f -wave pairing.

is determined by the self-consistent condition

$$\Sigma = -\frac{\Gamma}{g - c\sigma_3 g^{-1}\sigma_3}, \quad (28)$$

where $\Gamma = n_i/\pi\mathcal{N}_0$ is the scattering rate with n_i and \mathcal{N}_0 being the density of impurities and the DOS at the Fermi energy, respectively, $c = \cot \delta$ with δ being the scattering phase shift, and g is the normalized on-site Green's function

$$g = \frac{1}{\pi\mathcal{N}_0} \int \frac{d^2\mathbf{k}}{(2\pi)^2} G(\mathbf{k}, i\omega_n). \quad (29)$$

It is straightforward to verify that the σ_3 component of g is absent by particle-hole symmetry, and so are the $\sigma_{1,2}$ components in the case of non- s -wave pairing, justifying the *a priori* assumptions. Similar self-consistent equations holds for the retarded and advanced Green's functions, and are used in the realistic calculations via the spectral representation,

$$G(\mathbf{k}, i\omega_n) = \frac{1}{2\pi i} \int \frac{G^A(\mathbf{k}, \omega) - G^R(\mathbf{k}, \omega)}{i\omega_n - \omega} d\omega. \quad (30)$$

This is substituted into Eqs.(6) and (9) to calculate the Raman spectra in the presence of impurities. [12] Vertex corrections have been ignored, and are not expected to affect the conclusions significantly.

We first discuss the effect of unitary limit ($c = 0$). Fig.3(a) and (c) show the Raman spectra for s - and $p_x + ip_y$ -wave pairing under various values of the scattering rate Γ . For the s -wave pairing, the Raman spectra remains forbidden below the PBP at $\omega = 2\Delta_F$. Impurity scattering merely changes slightly the spectra above the peak. This is easily understood from the behavior of the DOS plot in Fig.3(b), where impurity does not induce intra-gap quasi-particles, consistent with the Anderson theorem. The slight change in the Raman spectra

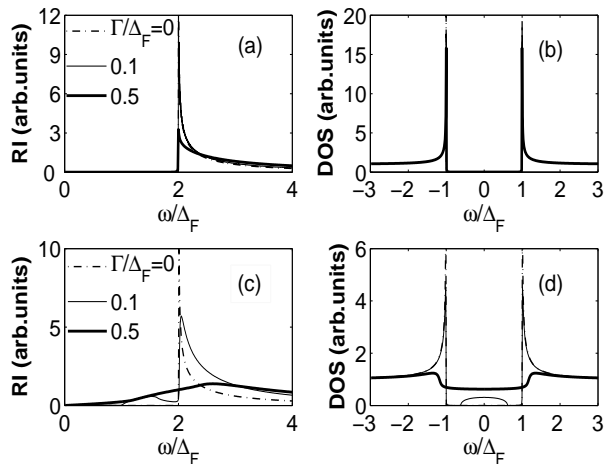


FIG. 3: The electronic Raman spectra for (a) s - and (c) $p_x + ip_y$ -wave pairing in the unitary limit for various values of the scattering rate. The corresponding DOS are shown for (b) s - and (d) $p_x + ip_y$ -wave pairing.

is due to the slight change in the DOS above the gap energy. The situation is quite different in Fig.3(c), where the Raman spectra is induced below the PBP. This can again be understood from the DOS induced by impurities in Fig.3(d). While there is a full gap in the clean limit, an impurity band is induced near the Fermi energy for small Γ . This is due to the nontrivial intrinsic phase of the $p_x + ip_y$ -wave pairing function. During impurity scattering, the quasi-particles experience a change of the intrinsic phase. It is shown elsewhere that by such an effect a single unitary impurity can induce an Andreev bound state, [13] and the bound states from a distribution of impurities can therefore form an impurity band. The scattering of quasi-particles by the light from the impurity band (below the Fermi energy) to the gap edge (above the Fermi energy) contributes most significantly to the Raman absorption below the PBP. This also explains the hump with a pseudo-threshold at $\omega = \Delta_F$. For very large Γ , the intra-gap is filled with induced DOS and accordingly the Raman spectra varies smoothly below $2\Delta_F$. We add that the Raman spectra for $d_{x^2-y^2} + id_{xy}$ -wave pairing behaves similarly to the $p_x + ip_y$ -wave pairing under a similar mechanism, and are not shown here for brevity.

Fig.4(a) shows the Raman spectra in the unitary limit for f -wave pairing. Although the PBP is lowered with increasing scattering rate, the low energy part is hardly changed. This implies a universal low energy Raman spectra in this case, to which we shall return shortly. The DOS is plot in Fig.4(b). In the absence of impurities, the DOS is linear at low energy, and impurities again induce low energy states. However, the impurity band is different from that in the $p_x + ip_y$ -wave case, in that this band connects smoothly to the higher energy DOS. This

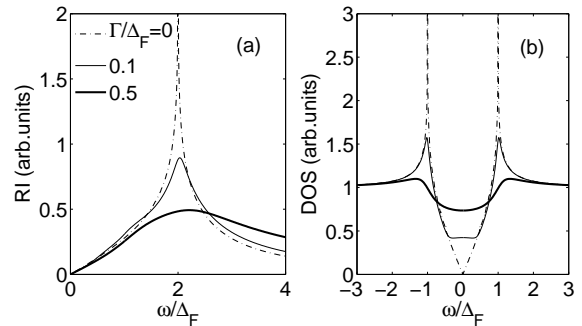


FIG. 4: (a) The electronic Raman spectra for f -wave pairing in the unitary limit. (b) The corresponding DOS.

explains the absence of new humps below the PBP in the Raman spectra. The universal low energy Raman spectra deserves further scrutiny. For a low scattering rate Γ , this can be proved exactly. From the CPA self-consistent equation the retarded self-energy $\Sigma^{A,R} = \pm i\eta\sigma_0$ in the low energy limit, where $\eta \sim \sqrt{\Gamma\Delta_F}$. If this is substituted into Eqs.(30) and (6), we find after some algebra that for $\omega \ll \Delta_F$ the Raman spectra is given by $-\text{Im}\chi(i\nu_n \rightarrow \omega + i0^+) = \alpha\omega\gamma^2/v_Fv_\Delta$, where α is a constant, $\gamma^2 = \langle\gamma_{\mathbf{k}}^2\rangle_F$ is the average square of the Raman vertex on the Fermi surface, v_F is the Fermi velocity and $v_\Delta = |\nabla_{\mathbf{k}}\Delta_{\mathbf{k}}|_{\mathbf{k}=\mathbf{k}_n}$ is the gap velocity at the six nodal points \mathbf{k}_n on the Fermi surface. The result is tied to the existence of nodal quasi-particles. The universal behavior in the Raman spectra is reminiscent to the universal conductivity discovered in the literature for $d_{x^2-y^2}$ -wave pairing in the cuprate superconductors.[14]

We have also considered general values of the inverse scattering strength c . The conclusion does not change for the s -wave case. The Raman spectra for $p_x + ip_y$ -wave case is shown in Fig.5(a) for various values of c . Fig.5(b) is the corresponding DOS. It is seen that near the Born limit, the center of the impurity band shifts away from the Fermi energy, causing a corresponding change in the Raman spectra. The Raman spectra for f -wave case is shown in Fig.5(c), and the DOS in Fig.5(d). Here no impurity band is formed in the Born limit, and the zero-energy DOS increases gradually with decreasing c . Interestingly this does not cause a change in the low energy limit of the Raman spectra. The reason is that for any values of c , as long as the resulting self energy is independent of energy in the low energy limit, the mechanism of universal Raman spectra applies as described above.

In summary, we developed a theory of electronic Raman scattering in superconductors on triangle lattices, with possible application to the cobalt oxide superconductors. The Raman response is shown to be independent of the light polarization configuration. However, in the case of s -wave pairing the absorption is forbidden below the PBP in the clean system as well as in the pres-

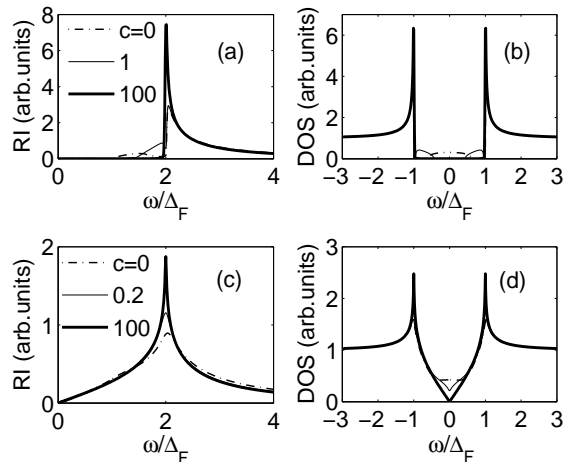


FIG. 5: The electronic Raman spectra for (a) $p_x + ip_y$ - and (c) f -wave pairing with $\Gamma/\Delta_F = 0.1$ and various values of c . The corresponding DOS are shown for (b) $p_x + ip_y$ - and (d) f -wave pairing.

ence of impurity scattering; in the cases of $p_x + ip_y$ - and $d_{x^2-y^2} + id_{xy}$ -wave pairing the absorption below the PBP is forbidden in the clean system, but can be induced by impurities; and finally in the case of nodal f -wave pairing there exists a universal low energy Raman response in the low energy limit for weak scattering rates. These features, combined with another probe of singlet versus triplet pairing, can be used to identify the relevant pairing symmetries unambiguously.

We thank Qing-Ming Zhang for useful discussions. This work was supported by NSFC 10204011, 10429401 and 10021001, the Fok Ying Tung Education Foundation No.91009, and the Ministry of Science and Technology of China (973 project No: 2006CB601002).

- [1] See, *e.g.*, T. P. Devereaux, D. Einzel, B. Stadlober, R. Hackl, D. H. Leach and J. J. Neumeier, Phys. Rev. Lett. **72**, 396(1994); T. P. Devereaux, D. Einzel, Phys. Rev. B **51**, 16336 (1995).
- [2] K. Takada, H. Sakurai, E. Takayama-Muromachi, F. Lzumi, Ruben A. Dilanian and T. Sasaki Nature(London) **422**, 53 (2003).
- [3] G. Baskaran, Phys. Rev. Lett. **91**, 097003 (2003); Qiang-Hua Wang, Dung-Hai Lee, and P. A. Lee, Phys. Rev. B **69**, 092504 (2004); B. Kumar, B. S. Shastry, Phys. Rev. B **68**, 104508(2003).
- [4] A. Tanaka and X. Hu, Phys. Rev. Lett. **91**, 257006 (2003).
- [5] K. Kuroki, Y. Tanaka, and R. Arita, Phys. Rev. Lett. **93**, 077001 (2004); M. D. Johannes, I. I. Mazin, D. J. Singh, and D. A. Papaconstantopoulos, Phys. Rev. Lett **93**, 097005 (2004); M. Mochizuki, Y. Yanase, and M. Ogata, Phys. Rev. Lett. **94**, 147005 (2005).
- [6] M. Kato, C. Michioka, T. Waki, K. Yoshimura, Y. Ihara, K. Ishida, H. Sakurai, E. Takayama-Muromachi, K. Takada and T. Sasaki, Physica B **359**, 482 (2005).
- [7] Y. Kobayashi, M. Yokoi, and M. Sato, J. Phys. Soc. Jpn. **72**, 2161 (2003); *ibid* **72**, 2453 (2003).
- [8] T. Fujimoto, Guo-qing Zheng, Y. Kitaoka, R. L. Meng, J. Cmaidalka and C. W. Chu, Phys. Rev. Lett. **92**, 047004(2004); K. Ishida, Y. Ihara, Y. Maeno, C. Michioka, M. Kato, K. Yoshimura, K. Takada, T. Sasaki, H. Sakurai, and E. Takayama- Muromachi, J. Phys. Soc. Jpn. **72**, 3041 (2003).
- [9] R. Jin, B. C. Sales, P. Khalifah, D. Mandrus, Phys. Rev. Lett. **91**, 217001 (2003); G. Cao, C. Feng, Y. Yu, W. Lu, J. Shen, M. Fang, and Z. Xu, J. Phys. Condens. Matt. **15**, L519 (2003); H. D. Yang, J. Y. Lin, C. P. Sun, Y. C. Kang, C. L. Huang, K. Takada, T. Sasaki, H. Sakurai, and E. Takayama-Muromachi, Phys. Rev. B **71**, 020504(R) (2005).
- [10] D. J. Singh, Phys. Rev. B **61**, 13397(2000).
- [11] A. Abrikosov and V. M. Genkin, Zh. Eksp. Teor. Fiz. **65**, 842(1973) [Sov. Phys. JETP **38**, 417 (1974)].
- [12] T. P. Devereaux, Phys. Rev. Lett. **74**, 4313 (1995).
- [13] Qiang-Hua Wang and Z. D. Wang, Phys. Rev. B **69**, 092502 (2004).
- [14] P. A. Lee, Phys. Rev. Lett. **71**, 1887 (1993); A. C. Durst and P. A. Lee, Phys. Rev. B **62**, 1270 (2000).

[1] See, *e.g.*, T. P. Devereaux, D. Einzel, B. Stadlober, R. Hackl, D. H. Leach and J. J. Neumeier, Phys. Rev. Lett.